Limiting factor of defect-engineered spin-filtering effect at room temperature

Y. Puttisong, I. A. Buyanova, and W. M. Chen
Department of Physics, Chemistry and Biology, Linköping University, S-581 83 Linköping, Sweden
(Received 3 February 2014; revised manuscript received 25 April 2014; published 12 May 2014)

We identify hyperfine-induced electron and nuclear spin cross-relaxation as the dominant physical mechanism for the longitudinal electron spin relaxation time (T_1) of the spin-filtering Ga_i^{2+} defects in GaNAs alloys. This conclusion is based on our experimental findings that T_1 is insensitive to temperature over 4–300 K, and its exact value is directly correlated with the hyperfine coupling strength of the defects that varies between different configurations of the Ga_i^{2+} defects present in the alloys. These results thus provide a guideline for further improvements of the spin-filtering efficiency by optimizing growth and processing conditions to preferably incorporate the Ga_i^{2+} defects with a weak hyperfine interaction and by searching for new spin-filtering defects with zero nuclear spin.

DOI: 10.1103/PhysRevB.89.195412 PACS number(s): 85.75.−d, 72.25.Rb, 78.20.Ls

Control of electron and nuclear spins at impurities and defects in semiconductors has attracted a considerable research interest due to their long spin relaxation times and well-defined spin states, desirable for applications in spintronics and spin-based quantum computation [1–5]. Two outstanding examples of such impurities and defects, regarded as being among the most promising candidates for scalable spin qubits, are the P donor in Si [6] and the nitrogen-vacancy (NV) center in diamond [7]. Recently Ga_i^{2+}-interstitial defects in Ga(In)NAs alloys have been shown to exhibit an extraordinary spin-filtering effect (see Fig. 1), which is capable of transforming the nonmagnetic semiconductors into an efficient spin filter and spin amplifier at room temperature (RT) [8,9]. It was further shown that a sizable nuclear spin polarization of the Ga_i^{2+} defects can be obtained at RT [10]—the first demonstration in a solid via spin-polarized conduction electrons. Again, a long spin relaxation time of the electron bound at the spin-filtering defects, which ought to be longer than that of conduction electrons, is crucial. Therefore, the key to the success of the aforementioned defect-enabled spin functionalities, whether they are spin qubits or spin filters/amplifier, is to control electron spin relaxation of the concerned impurities and defects. This is especially important at RT if the resulting spintronic devices and quantum computers are to be functional at RT for practical applications. For this, identification of the dominant mechanism for electron spin relaxation of the defects at RT becomes essential. Such studies can also pave the way for possible strategies to improve efficiency of spin functionalities by tailoring materials and physical parameters.

Electron spin relaxation is commonly described by a longitudinal spin-relaxation time T_1 representing an irreversible loss of spin projection on the direction of spin alignment and a spin decoherence time T_2 for loss in phase coherence of the transverse spin component. T_1 determines efficiency of classical information storage and processing. For example, it controls the efficiency of the RT defect-enabled spin filter/amplifier and optically read-out spin detector [8,9,11]. T_1 is also expected to set an upper limit for T_2, which is relevant to quantum information processing, e.g., it constrains the minimum gate operations for quantum error correction protocol [7]. Temperature dependence of T_1 for impurities and defects in semiconductors has been investigated in the past with the aid of electron spin resonance [12]. For a paramagnetic center with a concentration lower than 10^{16} cm^{-3}, where a spin-spin interaction between centers is negligible, earlier experimental and theoretical studies revealed two major types of spin relaxation [12–16]. One is related to spin-lattice relaxation (SLR) involving spin-orbit coupling (SOC), in which fluctuation of electrostatic potential induced by electron-phonon interactions causes electron spin flips via SOC. Depending on types of phonon interactions, T_1 exhibits characteristic and strong temperature dependence [12]. For example, the Orbach-type relaxation process that requires resonance coupling between the ground and excited states via local phonons has an exponential dependence of temperature [12,16]. The other type of spin relaxation refers to a cross relaxation between spin species, such as that between electron and nuclear (e-n) spins of a center promoted by a hyperfine interaction (HFI) [12,14]. In this case, T_1 is expected to be insensitive to temperature in zero magnetic field. Generally speaking, as SLR drastically accelerates with increasing temperature due to participation of phonons, they are commonly believed to be the dominant mechanism for T_1 at RT. For example, while SLR and HFI can equally contribute to T_1 at liquid He temperature, T_1 of shallow donors in Si is dominated by SLR at elevated temperatures [15]. For the NV center in diamond, SLR, including Orbach and Raman phonon processes, dominates in T_1 at 100–500 K [17–20].

The aim of this work is to determine the dominant physical mechanism for electron spin relaxation of the spin-filtering Ga_i^{2+} defects in GaNAs by closely examining temperature dependence of T_1 in Hanle-effect measurements. Furthermore, we intend to identify the microscopic origin of the observed spin relaxation by correlating T_1 with the exact configurations of the Ga_i^{2+} defects present in the material, as revealed by optically detected magnetic resonance (ODMR) [21]. Through these studies, we hope to single out the dominant factor in determining electron spin relaxation and to find a pathway to suppress it by varying growth and treatment conditions, thereby improving efficiency of the defect-engineered spin functionalities.

The studied samples are a set of undoped GaNAs alloys grown at 390–580 °C by molecular beam epitaxy on a (001) GaAs substrate, as listed in Table I. They were representative

 ©2014 American Physical Society

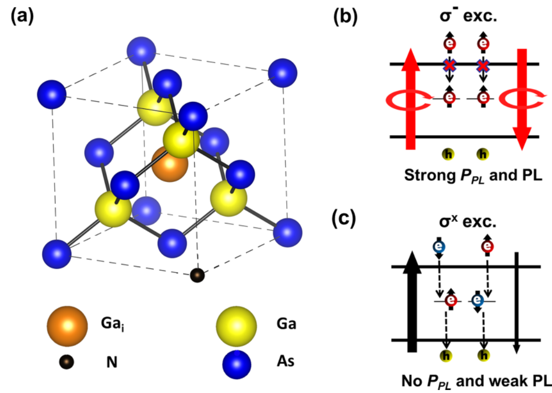

FIG. 1. (Color online) (a) Atomic structure of a Ga_i defect in GaNAs, for example, a Ga_i residing on the T_d site surrounded by the group-III sublattice. The exact atomic structures of the spin-filtering Ga_i defects studied in this work are still unknown in terms of their exact locations and their neighboring atoms. Therefore, the position of the N atom is for illustrative purposes and does not indicate its actual location. (b) Schematic illustration of the defect-engineered spin-filtering effect via SDR under σ^- excitation. The band-to-band optical transition should exhibit strong optical polarization, reflecting spin polarization of CB electrons, and stronger intensity as compared with the case (c) under σ^X excitation without the spin-filtering effect.

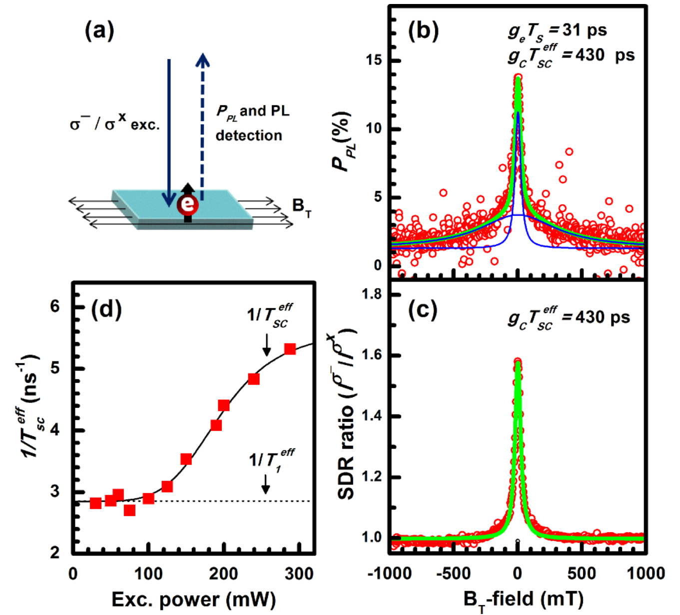

FIG. 2. (Color online) (a) A schematic picture of the Hanle measurements performed in this work. Hanle curves obtained at RT by monitoring P_{PL} (b) and SDR ratio $I^{\sigma^-}/I^{\sigma^X}$ (c). The solid lines are the fitting curves assuming two (b) or one (c) Lorentzian line(s), with the former being a sum of the Hanle curves for CB electrons (denoted by the thin broad line) and the defect electrons (the thin narrow line). (d) T_{SC}^{eff} as a function of optical excitation power, which approaches T_1^{eff} at the lowest excitation power.

of the alloy prepared under various growth and treatment conditions, leading to distinctly different relative concentrations of different configurations of Ga_i^{2+} defects, such that their effects on spin-filtering efficiency could be examined. Hanle measurements were performed in a Voigt configuration under optical orientation conditions [22,23] [see Fig. 2(a)]. Electron spins were oriented by circularly polarized laser light along the direction normal to the sample surface but perpendicular to a transverse magnetic field (B_T). Photoluminescence (PL) signals were detected in a back-scattering geometry by a cooled Ge detector integrated with a monochromator. ODMR measurements were done at 3–6 K with a microwave frequency either in X-band (∼9.2 GHz) or in Q-band (∼34 GHz), under optical excitation with a wavelength of 835–900 nm. ODMR signals, corresponding to PL intensity changes induced by microwaves under magnetic-resonance conditions [21], were detected by a cooled Ge detector through properly selected optical band-pass filters.

The basic principle of the defect-engineered spin-filtering effect is schematically illustrated in Figs. 1(b) and 1(c). Under circularly polarized optical excitation (e.g., σ^-), even a slight spin imbalance of conduction band (CB) electrons can lead to dynamic spin polarization of the electrons localized at the spin-filtering defects via spin-dependent recombination (SDR) that drives both CB and defect electrons toward the same spin orientation [8]. The resulting spin-polarized defects can subsequently only capture and deplete CB electrons of the opposite spin orientation, thereby enhancing spin polarization of CB electrons and thus optical polarization (P_{PL}) of the band-to-band (BB) PL transition between CB electrons and valence band (VB) holes. At the same time, the concentration of free carriers, thus the BB PL intensity, can also increase due to the spin blockade of competing carrier recombination via the defects, as compared to the case under linearly polarized excitation (σ^x) when SDR is deactivated [Fig. 1(c)]. Therefore, the effect of the spin-filtering effect can be measured by the so-called SDR ratio defined by $I^{\sigma^-}/I^{\sigma^X}$. Here I^{σ^-} and I^{σ^X} denote the total PL intensity under σ^- and σ^x excitation,

TABLE I. Details of the studied GaNAs samples. The parameters g_C^x, A^x, and α^x were determined by the spin Hamiltonian analysis of the ODMR results. $g_C^A = 2.01$, $g_C^B = 2.01$, $g_C^C = 2.00$, $\langle A^A \rangle = 0.081$ cm^{-1}, $\langle A^B \rangle = 0.131$ cm^{-1}, and $\langle A^C \rangle = 0.069$ cm^{-1}.

Samples		T_g(°C)	$Ga_i^{2+} - A$ α^A	$Ga_i^{2+} - B$ α^B	$Ga_i^{2+} - C$ α^x
I	$GaN_{0.026}$ $As_{0.974}$ epilayer	390	0.58	0.42	–
II	$GaN_{0.018}$ $As_{0.982}$/GaAs MQWs: $L_Z = 7$ nm	580	–	–	1.00
III	$GaN_{0.016}$ $As_{0.984}$/GaAs MQWs: $L_Z = 5$ nm	420	0.35	0.20	0.45
IV	$GaN_{0.013}$ $As_{0.987}$ epilayer	420	0.69	0.31	–
V	$GaN_{0.021}$ $As_{0.979}$ epilayer[a]	450	–	–	1.00

[a]*In situ* annealed at 700 °C for 3 minutes.

respectively. By measuring the SDR ratio as a function of B_T that depolarizes electron spins, the resulting Hanle curves provide information on the electron spin lifetime of the defects responsible for the spin-filtering effect.

In Fig. 2(b), we show a representative Hanle curve obtained at RT from the studied GaNAs alloys by monitoring the polarization of the BB PL transition between CB electrons and VB holes under circularly polarized optical excitation. The PL polarization degree is defined by $P_{PL} = (I_{\sigma^+} - I_{\sigma^-})/(I_{\sigma^+} + I_{\sigma^-})$, where I_{σ^+} and $I_{\sigma^-}$are the intensities of σ^+ and σ^- circularly polarized components of the BB PL emission, respectively. When only the BB PL involving heavy holes is detected, P_{PL} is one-to-one correlated with the spin polarization of CB electrons (P_e) with $P_e = -P_{PL}$ [23]. In our case, due to a contribution of the BB PL emission involving the light-holes [8], the actual degree of CB electron spin polarization should be larger than the measured degree of optical polarization in their absolute values. The observed quenching of P_{PL} (thus P_e) with increasing transverse magnetic field B_T can be ascribed to the well-known Hanle effect, in which optically generated electron spins can be depolarized in an applied B_T due to a Larmor precession of the electron spins about the field direction [22,23]. As P_e of CB electrons and the spin polarization of the electrons at the Ga_i^{2+} defects (denoted by P_C) are interconnected via the SDR process and the resulting spin filtering and spin blockade, the observed Hanle curve should be described by a system of two coupled electron spin species [9,24,25]. For simplicity, it can be approximately described as consisting of two Lorentzian curves with one for CB electrons and the other for the defect electrons, as shown by the thin solid curves in Fig. 2(b) [22]. To remove the contribution from the CB electrons and thereby increase the accuracy in determining the spin lifetime of the defect electrons, we choose to study the Hanle effect on the SDR. This is because a significant increase in the PL intensity can only be accomplished when the electron spins at the Ga_i^{2+} defects are polarized, leading to a spin blockade of the carrier recombination via the defects that competes with the BB PL transition. The resulting Hanle curve by monitoring $I^{\sigma^-}/I^{\sigma^X}$ is shown in Fig. 2(c), which only consists of a single Lorentzian component originated from the defect electrons. Consequently, the Hanle curve by monitoring the SDR ratio is much simpler and can be fitted by a single Lorentzian line, with a linewidth determined only by the defect electron spin life-time. The half-width field of the Hanle curve is determined by the relation $B_{1/2} = \hbar/(\mu_B g_C T_{SC})$ [22,23]. Here, $\hbar$ is the Planck constant, μ_B is the Bohr magneton, and g_C is the g factor of the defect electrons. T_{SC} is the spin lifetime of the electrons at the Ga_i^{2+} defect, taking into account all events that disrupt the Larmor procession. It is determined by the relation $1/T_{SC} = 1/\tau + 1/T_1$. Here τ is the electron lifetime of the paramagnetic Ga_i^{2+} defect, which is controlled by the capture of a second electron [8–11,24,25] and should therefore be inversely proportional to the concentration of the CB electrons (thus optical excitation density). Under an extremely low excitation density, when $\tau \gg T_1$, $T_{SC} \to T_1$ such that T_1 can be determined by measuring $B_{1/2}$ [22–25]. This is clearly confirmed by our experimental results shown in Fig. 2(d), where T_{SC}^{eff} and T_1^{eff} are used to represent their

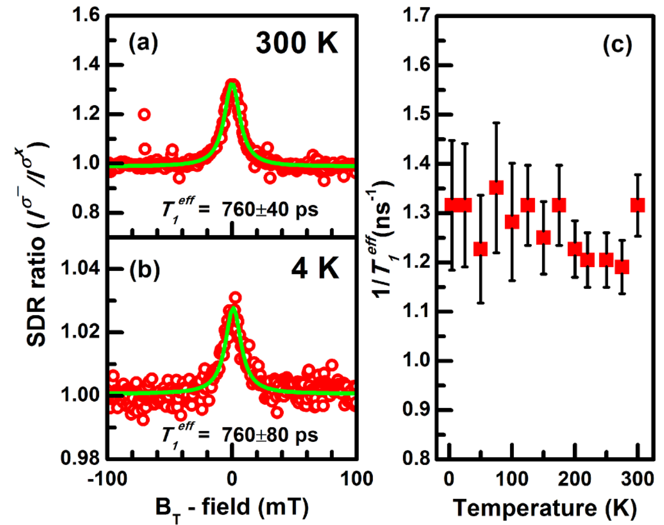

FIG. 3. (Color online) (a), (b) Hanle curves (open circles) obtained from Sample V at 300 K and 4 K by monitoring $I^{\sigma^-}/I^{\sigma^X}$. The solid lines are fitting curves assuming a Lorentzian lineshape. (c) $1/T_1^{\text{eff}}$ as a function of measurement temperature. The error bars are deduced from the uncertainty in the fitting procedure. All the measurements were done under very weak optical excitation.

effective values in view of possible contributions from several Ga_i^{2+} defects in the same sample, as revealed from our ODMR studies.

The above approach has enabled us to conduct a careful and systematic study of T_1^{eff} as a function of measurement temperature in all studied GaNAs samples. Representative Hanle curves measured at 300 K and 4 K under weak optical excitation are displayed in Figs. 3(a) and 3(b). By using the value of $g_C \approx 2$ determined from our ODMR studies (see below), we deduce $T_1^{\text{eff}} = 760$ ps at both 300 K and 4 K for Sample V. A complete temperature dependence of T_1^{eff} from 4 K to RT is shown in Fig. 3(c), demonstrating a temperature-independent behavior of T_1^{eff}. As spin-spin interactions between nearby defects or between CB and defect electrons are expected to play a negligible role here due to low densities of the highly localized Ga_i^{2+} defects ($\leqslant 10^{16}$ cm^{-3}) [24,26] and photogenerated CB electrons, the observed temperature independence of T_1^{eff} is thus indicative of an HFI-mediated electron spin relaxation at the Ga_i^{2+} defects. This is found to be a common property in all of the studied GaNAs samples. The exact value of T_1^{eff}, on the other hand, varies between samples. For example, $T_1^{\text{eff}} = 350$ ps is deduced in Sample I, whereas in Sample II $T_1^{\text{eff}} = 800$ ps, as shown in Figs. 4(a) and 4(b).

To shed light on the microscopic origin of this variation in T_1^{eff}, ODMR was employed to identify the exact configurations of the Ga_i^{2+} defects present in each of the studied GaNAs samples. As examples, typical ODMR spectra from Samples I and II are displayed by the open circles in Figs. 4(c) and 4(d), respectively. They were analyzed by the spin Hamiltonian:

$$H = \mu_B g_C \overrightarrow{B} \cdot \vec{S}_C + A\vec{I} \cdot \vec{S}_C. \quad (1)$$

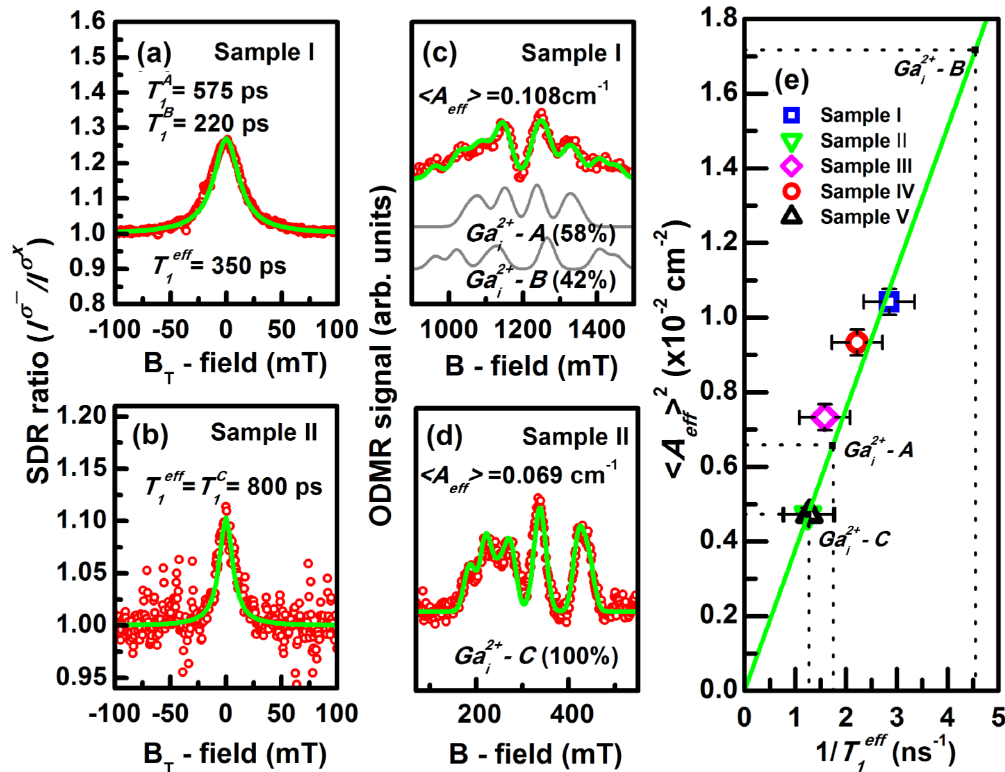

FIG. 4. (Color online) (a), (b) Hanle curves (open circles) obtained at RT from Sample I and II. The solid lines are the simulation curves obtained by a best fit of the coupled rate equations to the experimental data, with the specified fitting parameters of T_1^x. $T_1^{\rm eff}$ is estimated from the effective Hanle width. (c), (d) ODMR spectra of the Ga_i^{2+} defects obtained at 4 K from Samples I and II. The solid lines are the simulation curves obtained by a best fit of the spin Hamiltonian Eq. (1) to the experimental data. The involved configurations of the Ga_i^{2+} defects are given in (c) and (d), together with the degrees of their contributions and the resulting $\langle A_{\rm eff}\rangle$. The microwave frequencies used in ODMR are 33.92 GHz in (c) and 9.27 GHz in (d). (e) $\langle A_{\rm eff}\rangle^2$ as a function of $1/T_1^{\rm eff}$, with each symbol representing a specific sample. The solid line is a linear fitting following the Fermi-golden rule. The dotted lines mark the associated parameters of each Ga_i^{2+}configuration, obtained from the rate equation and spin Hamiltonian analysis of the experimental data.

The first and second term represent the electronic Zeeman interaction and HFI, respectively, with $\vec{S}_C$ ($\vec{I}$) being the electron (nuclear) spin operator and A being the HFI parameter. From the best fit to the experimental data, shown by the solid curves in Figs. 4(c) and 4(d), three different configurations of the Ga_i^{2+} defects can be identified and are denoted as Ga_i^{2+}-A, Ga_i^{2+}-B, and Ga_i^{2+}-C [26]. The most distinct difference between these variations of the Ga_i^{2+} defects is their HFI parameters. The analysis takes into account contributions from both naturally abundant Ga isotopes, i.e., $^{69}Ga_i$ and $^{71}Ga_i$, with the ratio of 60.1%/39.9% for their natural abundance and the ratio of 0.787 for their nuclear magnetic moment. The spin Hamiltonian parameters determined for each configuration of the Ga_i^{2+} defects are given in Table I. The A parameter and g_C factor for all Ga_i^{2+} configurations are isotropic, revealed from angular-dependent studies of the ODMR signals, concluding that the wavefunction of the electron localized at the defects is s-like [8,26]. The relative contributions of these Ga_i^{2+} defects in the ODMR spectra from each sample are denoted by α^x in Table I. Here $x = A$, B, and C for $Ga_i^{2+} - A$, $Ga_i^{2+} - B$, $Ga_i^{2+} - C$, and $\sum_{x=A,B,C}\alpha^x = 1$. It is clear from Table I and Figs. 4(c) and 4(d) that a large variation of α^x can be found between samples. In agreement with our earlier studies, our results show that the introduction of these different forms of the Ga_i^{2+} defects critically depends on growth conditions and post-growth treatments. For example, $Ga_i^{2+} - C$ was preferably incorporated in the alloy under growth at a high temperature or after postgrowth thermal annealing, represented by Samples II and V. The untreated samples grown at low temperatures (Samples I and IV) represent the cases when the dominant Ga_i^{2+} defects are $Ga_i^{2+} - A$ and $Ga_i^{2+} - B$. Sample III, on the other hand, shows a situation when all three defects are present. The quantum well width (L_Z) does not play any significant roles in the relative contributions of different Ga_i^{2+} defects, known from our previous studies [27]. (Sample II and III were chosen here to demonstrate the effect of growth temperature, not L_Z.)

To correlate the HFI strength obtained from the ODMR study with $T_1^{\rm eff}$ from the Hanle measurements, an effective HFI parameter of the Ga_i^{2+} defects in each sample is estimated by $\langle A_{\rm eff}\rangle = \sum_{x=A,B,C}\alpha^x\langle A^x\rangle$, where $\langle A^x\rangle = 60.1\,\% * A^x(^{69}Ga_i^{2+}) + 39.1\,\% * A^x(^{71}Ga_i^{2+})$ is the effective HFI parameter of the specific Ga_i^{2+}-X defect that is a weighted average over the two Ga isotopes. The estimated $\langle A_{\rm eff}\rangle$ values for all samples are plotted as the open symbols in Fig. 4(e) as a function of $T_1^{\rm eff}$ determined from the Hanle widths. Despite the approximation, a direct correlation between $T_1^{\rm eff}$ and

$\langle A_{\rm eff}\rangle$ is apparent. They closely follow the relation $1/T_1^{\rm eff} \propto \langle A_{\rm eff}\rangle^2$, which is expected only when $T_1^{\rm eff}$is dominated by e-n spin cross-relaxation mediated by the nonsecular HFI term $\frac{A}{2}(I_+S_- + I_-S_+)$. This correlation thus provides further support for the dominant role of the HFI in $T_1^{\rm eff}$of the Ga_i^{2+} defects.

Strictly speaking, a Hanle curve with simultaneous contributions from several Ga_i^{2+} defects with different HFI strengths and thus T_1 values may not exactly follow a simple Lorentzian lineshape. To more precisely analyze the experimental Hanle curves and deduce T_1 for each defect configuration, we employ the following coupled rate equations that explicitly take into account of the contributions from all Ga_i^{2+} defects present in each sample:

$$\frac{dn}{dt} = G - \frac{\gamma_e}{2}\left[\sum_{x=A,B,C}\left(nN_1^x - 4\vec{S}\cdot\vec{S}_C^x\right)\right]$$

$$\frac{d\vec{S}}{dt} = \frac{G}{2}\vec{P}_e^{\,i} - \frac{\gamma_e}{2}\left[\sum_{x=A,B,C}\left(\vec{S}N_1^x - n\vec{S}_C^x\right)\right] - \frac{\vec{S}}{\tau_S} - \vec{S}\times\vec{\Omega},$$

$$\frac{d\vec{S}_C^x}{dt} = -\frac{\gamma_e}{2}\left(n\vec{S}_C^x - \vec{S}N_1^x\right) - \frac{\vec{S}_C^x}{T_1^x} - \vec{S}_C^x\times\vec{\Omega}_C^x, (x = A,B,C)$$

$$\frac{dp}{dt} = G - \gamma_h\sum_{x=A,B,C} pN_{\uparrow\downarrow}^x,$$

$$N_C^x = N_1^x + N_{\uparrow\downarrow}^x = \alpha^x N_C^{\rm total},$$

$$N_C^{\rm total} = \sum_{x=A,B,C} N_C^x, \quad \sum_{x=A,B,C}\alpha^x = 1. \quad (2)$$

Here, the superscript x ($x = A$, B, or C) denotes the configuration of the concerned Ga_i^{2+}-X defect. $\vec{S}$ and $\vec{S}_C^x$ are the spin operators of CB electrons and the electrons bound at the Ga_i^{2+}-X defect, respectively. G is the generation rate of CB electrons (n) and VB holes (p), which can be estimated from excitation photon density. $\vec{P}_e^i$ is the initial spin polarization of CB electrons generated by optical orientation without the spin-filtering effect. Its value can be obtained at a low excitation density before the defect-enabled spin filtering takes effect.N_1^x and $N_{\uparrow\downarrow}^x$ are the concentrations of Ga_i^{2+}-X (with one bound electron) and Ga_i^{+}-X (with two bound electrons after capture of a second electron by Ga_i^{2+}-X), respectively. N_C^x is the total concentration of the Ga_i-X defect, i.e., the sum of the concentrations of both Ga_i^{2+}-X and Ga_i^{+}-X charge states. It is a fraction of the total defect concentration, including all configurations of the Ga_i defects ($N_C^{\rm total}$), following the relation $N_C^x = N_1^x + N_{\uparrow\downarrow}^x = \alpha^x N_C^{\rm total}$, where α^x can be estimated from the relative ODMR signal intensity of $Ga_i^{2+} - X$. $\vec{\Omega} = g_e\mu_B\vec{B}/\hbar$ and $\vec{\Omega}_C^x = g_C^x\mu_B\vec{B}/\hbar$ are the Larmor frequencies of CB electrons (with a g factor, g_e) and the bound electrons at Ga_i^{2+}-X. γ_e and γ_h are the capture coefficients of CB electrons and VB holes by the defect center, respectively, which are assumed to be the same for all configurations of Ga_i defects with $\gamma_e/\gamma_h = 4$, as deduced from earlier studies [8]. τ_S is the spin relaxation time of CB electrons. Though the parameters of g_e and τ_S that are related to CB electrons may vary from sample to sample, their effect on the Hanle curve are expected to be only limited to the broad component arising from CB electrons when P_{PL} is monitored [see Fig. 2(b)]. They have little effect on the width of the narrow component in the Hanle curves that is related to the defect electrons, especially when the SDR ratio $I^{\sigma^-}/I^{\sigma^X}$ is monitored. For simplicity, we use $g_e = 1$ and $\tau_S = 150$ ps that were deduced from earlier studies [8,28]. $\gamma_e N_C^{\rm total}$ can be obtained by fitting the zero-field value of $I^{\sigma^-}/I^{\sigma^X}$ for each sample as a function of excitation density [8]. As α^x and g_C^x are known from the ODMR studies, T_1^x is left as the only fitting parameter that can affect the Hanle width under a low excitation density. From a best fit of the rate equations to the experimental data, T_1^x for each Ga_i^{2+}-X defect can therefore be determined, i.e., $T_1^A = 575$ ps, $T_1^B = 220$ ps, and $T_1^C = 800$ ps. The fitting Hanle curves using these parameters are shown by the solid lines in Figs. 4(a) and 4(b), in excellent agreement with the experimental data.

We should note that a perfectly linear relation between $1/T_1^x$ and $\langle A^x\rangle^2$ is found for all configurations of the Ga_i^{2+}-X defects with a ratio of $\frac{\langle A^x\rangle^2}{1/T_1^x} = 3.78$ ps $\cdot$ cm^{-2}, as shown in Fig. 4(e). In other words, the rate equation analysis further confirms that T_1^x of all Ga_i^{2+}-X defects is governed by e-n spin cross-relaxation. This finding thus provides a guideline to suppress electron spin relaxation at the Ga_i^{2+}-X defects, i.e., to select defects with a weaker or preferably vanishing HFI. For example, the HFI of Ga_i^{2+}-C is about twice as weak as that of Ga_i^{2+}-B. This yields $T_1^C \approx 4T_1^B$ and makes Ga_i^{2+}-C a more efficient spin-filtering defect than Ga_i^{2+}-B. Ga_i^{2+}-C is known to be preferably introduced in GaNAs alloys grown at high temperatures (e.g., Sample II) or has undergone postgrowth thermal annealing (e.g., Sample V). Unfortunately, these conditions are generally found to be accompanied by a reduction in the concentrations of the Ga_i^{2+} defects leading to a corresponding decreasing spin-filtering efficiency. Future research efforts are thus required to identify optimal growth and processing conditions for more efficient incorporation of Ga_i^{2+}-C or other weak-HFI configurations of the Ga_i^{2+} defects. Even better is to search for new spin-filtering defects with a core atom free of nuclear spins and thus with zero central HFI.

To quantify the effect of HFI on the spin-filtering effect, we have calculated the maximum achievable degree P_e of CB electron spin polarization as a function of the HFI parameter A with the aid of the same rate equation analysis described above. The simulation results shown in Fig. 5 show a clear trend of increasing P_e with decreasing A. The saturation value of P_e for each given defect concentration (N_C) is determined by the competing processes between spin relaxation and spin-dependent capture by the spin-filtering defects that are experienced by CB electrons. By increasing N_C that scales with the capture rate of CB electrons, the contribution of CB electron spin relaxation can be continuously reduced, leading to a further improvement in the spin-filtering efficiency such that P_e approaches 100%.

It is also interesting to note that the strict requirements for a spin-filtering defect (not limited to the studied Ga_i^{2+} defects) have simultaneously ensured that thermally activated

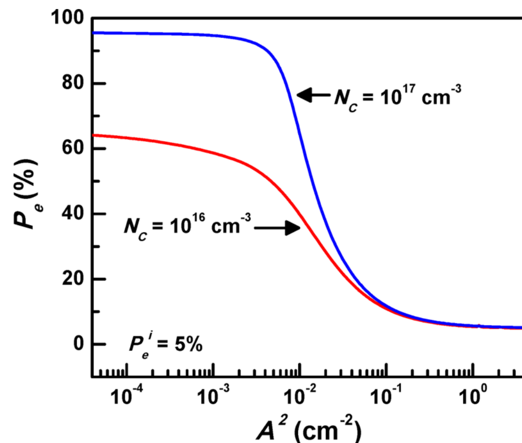

FIG. 5. (Color online) Spin polarization degree of CB electrons (P_e) as a function of the HFI parameter A, calculated by the coupled rate equation analysis described in Eq. (2). The simulations are performed with 5% of initial spin polarization of CB electrons (P_e^i), generated by optical orientation before the defect-enabled spin filtering takes effect, and two values of the defect concentration (N_C), as examples.

electron spin relaxation processes associated with SLR-SOC are strongly suppressed, leading to the observed vanishing contributions of these spin relaxation processes in the studied Ga_i^{2+} defects even at RT. The first of such requirements is a nondegenerate orbital state of the defect such that it can only be occupied by two electrons with opposite spin orientations dictated by the Pauli Exclusion Principle, as illustrated in Fig. 1(b). The orbital angular momentum of such a state should be quenched to the first order [28], as evident from the isotropic g_C, for all Ga_i^{2+} defects that are close to the electron g factor in free space. This strongly suppresses SOC and thus all SOC-induced SLR processes. Another requirement for a spin-filtering defect is the absence of excited states within the bandgap. Otherwise, CB electrons of both spin orientations would be captured by the defect as long as they are not in the same orbital state, and the spin-filtering effect would cease to function. The absence of real excited states of the defect prohibits, at the same time, all the spin relaxation processes associated with resonance phonon interactions between the ground and excited state, such as the Orbach-type process [12,16]. In a word, the strict requirements for a spin-filtering defect have elevated the importance of HFI in electron spin relaxation of the defect and consequently in the efficiency of the spin-filtering effect, which should be a focal point of future studies. In many ways, these requirements have also made spin-filtering defects excellent candidates for spin qubits, in which thermally activated SLR processes are largely suppressed such that a long electron spin relaxation time is possible even at RT (when spin-filtering defects with weak or zero HFI are selected).

In conclusion, we have identified e-n spin cross-relaxation as the dominant spin relaxation mechanism of the spin-filtering Ga_i^{2+} defects in the GaNAs alloy. This is supported by our experimental findings that T_1 is insensitive to measurement temperature over the wide range of 4–300 K, and it is closely correlated with the HFI strengths of the Ga_i^{2+} defects following the Fermi-golden rule. These results point to the direction toward further improvements of the spin-filtering efficiency either by optimizing growth and processing conditions to preferably incorporate the Ga_i defects with a weak HFI or by searching for new spin-filtering defects with zero nuclear spin. Furthermore, we suggest that spin-filtering defects may also be excellent candidates for spin qubits.

We thank C. W. Tu, L. Geelhaar, H. Riechert, and V. K. Kalevich for providing the samples. This work was supported by Linköping University through the Professor Contracts, Swedish Research council (Grant No. 621-2011-4254), Swedish Energy Agency, and Knut and Alice Wallenberg Foundation.

[1] S. A. Wolf, D. D. Awschalom, R. A. Buhrman, J. M. Daughton, S. von Molnár, M. L. Roukes, A. Y. Chtchelkanova, and D. M. Treger, Science **294**, 1488 (2001).
[2] I. Žutić, J. Fabian, and S. Das Sarma, Rev. Mod. Phys. **76**, 323 (2004).
[3] D. D. Awaschalom and M. F. Flatté, Nature Physics **3**, 153 (2007).
[4] *Semiconductor Spintronics and Quantum Computation*, edited by D. Awschalom, D. Loss, and N. Samarth (Springer-Verlag, Berlin, Heidelberg, 2002).
[5] *Handbook of Spintronic Semiconductors*, edited by W. M. Chen and I. A. Buyanova (Pan Stanford, Singapore, 2010).
[6] B. E. Kane, Nature **393**, 133 (1998).
[7] T. D. Ladd, F. Jelezko, R. Laflamme, Y. Nakamura, C. Morroe, and J. L. O'Brien, Nature (London) **464**, 45 (2010).
[8] X. J. Wang, I. A. Buyanova, F. Chao, D. Zhao, D. Lagarde, A. Balocchi, X. Maries, C. W. Tu, J. C. Harmand, and W. M. Chen, Nat. Mater. **8**, 198 (2009).
[9] Y. Puttisong, I. A. Buyanova, A. J. Ptak, C. W. Tu, L. Geelhaar, H. Riechert, and W. M. Chen, Adv. Mater. **25**, 738 (2013).
[10] Y. Puttisong, X. J. Wang, I. A. Buyanova, L. Geelhaar, H. Riechert, A. J. Ptak, C. W. Tu, and W. M. Chen, Nat. Commun. **4**, 1751 (2013).
[11] Y. Puttisong, I. A. Buyanova, L. Geelhaar, H. Riechert, and W. M. Chen, J. Appl. Phys. **111**, 07C303 (2012).
[12] *Electron Paramagnetic Resonance of Transition Ions*, edited by A. Abragam and B. Bleaney (Dover Publications, Inc., New York, 1986).
[13] D. Pines, J. Bardeen, and C. P. Slichter, Phys. Rev. **106**, 489 (1957).
[14] J. W. Culvahouse and F. M. Pipkin, Phys. Rev. **109**, 319 (1958).
[15] T. G. Castner, Jr., Phys. Rev. **130**, 58 (1963).
[16] C. B. P. Finn, R. Ocbach, and W. P. Wolf, Proc. Phys. Soc. (London) **77**, 261 (1960).

[17] D. A. Redman, S. Brown, R. H. Sands, and S. C. Rand, Phys. Rev. Lett. **67**, 3420 (1991).
[18] S. Takahashi, R. Hanson, J. van Tol, M. S. Sherwin, and D. D. Awschalom, Phys. Rev. Lett. **101**, 047601 (2008).
[19] J. Harrison, M. J. Sellars, and N. B. Manson, Diam. Relat. Mater. **15**, 586 (2006).
[20] A. Jarmola, V. M. Acosta, K. Jensen, S. Chemerisov, and D. Budker, Phys. Rev. Lett. **108**, 197601 (2012).
[21] W. M. Chen, Thin Solid Films **364**, 45 (2000).
[22] *Spin Physics in Semiconductors*, edited by M. I. Dyakonov (Springer, Berlin, Heidelberg, 2008).
[23] *Optical Orientation*, edited by F. Meier and B. P. Zakharchenya (North-Holland, Amsterdam, 1984).
[24] E. L. Ivchenko, V. K. Kalevich, A. Yu. Shiryaev, M. M. Afanasiev, and Y. Masumoto, J. Phys: Condens. Matter. **22**, 465804 (2010).
[25] V. K. Kalevich, A. Yu Shiryaev, E. L. Ivchenko, M. M. Afanasiev, A. Yu. Egorov, V. M. Ustinov, and Y. Masumoto, Physica B **404**, 4929 (2009).
[26] X. J. Wang, Y. Puttisong, C. W. Tu, A. J. Ptak, V. K. Kalevich, A. Yu. Egorov, L. Geelhaar, H. Riechert, W. M. Chen, and I. A. Buyanova, Appl. Phys. Lett. **95**, 241904 (2009).
[27] Y. Puttisong, X. J. Wang, I. A. Buyanova, H. Carrere, F. Zhao, A. Balocchi, X. Marie, C. W. Tu, and W. M. Chen, Appl. Phys. Lett. **96**, 052104 (2010).
[28] B. Monemar, U. Lindefelt, and W. M. Chen, Physica B **146**, 256 (1987).